Appl. Phys. A 30, 33–41 (1983)

Applied Physics A Solids and Surfaces

Subsurface Segregation and Diffusion of Carbon in Magnesium Oxide

H. Kathrein[1], H. Gonska[2], and F. Freund*

[1]Mineralogisches Institut, [2]Lehrstuhl Theoretische Chemie, Universität, D-5000 Köln 41, Fed. Rep. Germany

Received 26 February 1982/Accepted 24 September 1982

Abstract. Carbon dissolved in the (100) surface of MgO single crystals, grown by arc-fusion, was studied by x-ray photoelectron spectroscopy, XPS, between 80–920 K. In the complex C 1*s* spectrum observed the signal due to the carbon species contained in the MgO structure are distinguishable from those due to contamination. The XPS data support the conclusions, derived with a lesser depth resolution, from earlier $^{12}C(d,p)^{13}C$ concentration profile analysis [Wengeler et al.: J. Phys. Chem. Solids **43**, 59–71 (1982)] that the carbon in MgO strongly segregates into the subsurface zone. A typical bulk C concentration is 300 wt.-ppm, corresponding to about 1000 at.-ppm. The C concentration in the topmost 5–10 nm analyzed by XPS, however, may be as high as one C per two O. With increasing temperature the C concentration decreases. Upon cooling the C concentration rises in a reversible manner. The diffusion coefficient of carbon in MgO was determined by measuring the subsurface C concentration increase at different temperatures after Ar ion sputtering:

$D_{C/MgO} = 2 \times 10^{-9} \exp(-22.5 \pm 2.5/RT)\,[cm^2\,s^{-1}$ and $KJ \cdot mole^{-1}]$.

PACS: 61.70 Wp, 66.30 Jt, 79.60 Eq

Carbon-concentration depth-profile measurements using the $^{12}C(d,p)^{13}C$ nuclear reaction have been very substantial for understanding the behavior of dissolved carbon in densely packed oxides like synthetic MgO and CaO [1–4] and in natural mantle-derived olivines [5]. In addition gas evolution studies [6, 7] have provided important informations about the chemistry which takes place at the crystal surfaces when the dissolved carbon reacts with lattice oxygen, with co-dissolved hydrogen and even with the metal component to give CO_2, CO, a large variety of hydrocarbons and metallo-organics [5].

The $^{12}C(d,p)^{13}C$ method has the advantage of being a specific analytical tool for carbon analysis in oxide matrices. It provides information about total carbon and carbon concentration depth profiles. Interferences with other elements are rare or can be accounted for [8]. Its main drawback lies in the fact that the depth resolution achieved even under optimum conditions is rather poor, approximately 0.4 μm [4]. In order to learn more about the carbon concentration in the first atomic layers where the surface chemistry takes place, we choose photoelectron spectroscopy with x-rays for excitation, XPS. Unfortunately XPS is extremely sensitive to surface contamination with carbon. Special efforts have to be made to assess possible extraneous carbon sources and to distinguish the carbon species due to contamination from those inherent to the sample.

1. Experimental

The photoelectron spectrometer used in the present study, a modified LEYBOLD LHS-10 system which

* Present address: Department of Physics, Arizona State University, Tempe, AZ 85287, USA

0721-7250/83/0030/0033/$01.80

was pumped by turbo-molecular pumps providing an essentially hydrocarbon-free ultrahigh vacuum of the order of 10^{-8} Torr or better. The $MgK_{\alpha 1,2}$ radiation from the x-ray tube (10 kV and typically 39 mA) passed through a 5 μm thick Al window separating the x-ray tube vacuum from the main chamber [9]. The total energy resolution including the electron optics and the spherical 180° analyzer was about 1.3 eV.
The sample surface area "seen" by the spectrometer was 2×9 mm^2 with some slight contribution from the surrounding area. One sample at a time was mounted in a rectangular Cu dish on the horizontal sliding sample rod. The sample was changed between the measuring position and the preparation chamber, provided with a 3 kV argon sputtering gun. The temperature of the sample could be varied in a controlled manner between 80–920 K.

1.1. Samples

The MgO sample was a 3*N*-grade synthetic single crystal, $6 \times 6 \times 1$ mm^3, grown by arc-fusion by W. & C. Spicer Ltd., Cheltenham, England, optically transparent, as described earlier [4] with an average C content of the order of 300–350 wt.-ppm contained as atomically dissolved C in the lattice. A thin surface layer was removed from the cleaved (100) face by dry polish on α-Al_2O_3 impregnated polishing foil (3M Co, Minneapolis, Minnesota, USA), followed by chemical etching in 80% H_3PO_4 and rinsing with distilled water. The samples were sputtered at 300 K by Ar ions, 3 kV at 2×10^{-4} Torr for about 1 min at normal incidence corresponding to a dose of about 10 mCb/cm^2.
As a carbon standard a graphite single crystal from Sri Lanka was used, $10 \times 10 \times 1$ mm^3, cut normal to the (100) plane. It was etched, rinsed and sputtered in the same way as the MgO and olivine samples. After sputtering the graphite crystal was annealed at 900 K in UHV for 1 h in order to remove lattice strains and sputter-induced defects.

1.2. Data Collection

Carbon was analyzed by its C 1*s* signal around $E_b = 295$ eV, oxygen and magnesium by their O 1*s* and Mg 2*s* signals at about $E_b = 540$ eV and $E_b = 95$ eV, respectively. The sample surface was uniformely charged by +2 V with respect to ground. After introducing the samples into the preparation chamber and Ar sputtering they were subjected to different heat treatments while being in the measuring position. Heating was always relatively fast. 110, 220, 300, and 500 s to reach 500, 700, 800, and 900 K, respectively. Photoelectron spectra were usually recorded every 5 min. Kinetic measurements were extended over 3 h and more, especially at higher temperatures when no contamination layer could build up on the sample surfaces.
The XPS peak profiles were registered on a chart recorder and deconvoluted, if necessary, on a DUPONT Curve Analyzer assuming a minimum number of peak components with a constant half width of 2.3 eV and an experimentally adjusted peak shape which is closely Gaussian.

1.3. Quantitative Analysis with Special Reference to Carbon

In order to evaluate quantitatively the photoelectron spectra the sample is thought to be composed of infinitely thin layers of thickness dz. Each layer contains a concentration ϱ_z of the element to be analyzed in atoms per mole of the host lattice. Each layer contributes dN to the total intensity of the photoelectron peak. We can write [10]

$$dN = I_z \cdot T(E_{\text{kin}}, k^f, z) \cdot \varrho_z \cdot dz \cdot \frac{d\sigma}{d\Omega} \cdot \Omega(E_{\text{kin}}, z) \cdot D(E_{\text{kin}}), \quad (1)$$

where I_z is the x-ray quantum flux at z, $T(E_{\text{kin}}, k^f, z)$ is the probability of a primary photoelectron to leave the sample without energy losses in z-direction from a given depth z and with an angular spread k^f, $d\sigma/d\Omega$ is the differential cross section of the energy level under consideration, $\Omega(E_{\text{kin}}, z)$ the acceptance angle of the analyzer, and $D(E_{\text{kin}})$ the detector efficiency.
With the usual assumptions and a mean free path Λ of the photoelectrons integration of (1) yields

$$N = I_0 \cdot \Lambda(E_{\text{kin}}) \cdot \varrho \cdot A \frac{d\sigma}{d\Omega} \cdot \Omega \cdot D(E_{\text{kin}}), \quad (2)$$

where A is the effective sample surface. By comparison with a standard (index 0) the molar concentration ϱ in the sample (index s) can be obtained:

$$\varrho_s = \frac{N_s}{N_0} \frac{\Lambda_0(E_{\text{kin}})_0}{\Lambda_s(E_{\text{kin}})_s} \cdot \frac{A_0}{A_s} \cdot \varrho_0 . \quad (3)$$

The exact values for the loss-free escape depth of C 1*s* electrons from MgO and the reference graphite single crystal being not known, the ratio Λ_0/Λ_s can be different from unity. By setting $\Lambda_0 = \Lambda_s$, the absolute carbon concentrations calculated below may be wrong by a factor of 2 to at most 4. The relative carbon concentrations, however, remain unaffected by this neglect of matrix effects [11]. The carbon concentrations are given below in number of C atoms per O atoms in the analyzed layer of MgO.
The XPS method is sensitive to surface contamination even in the range of submonolayer coverage. This applies in particular to the analysis of carbon in the

sample. If the surface is covered by a contamination layer of thickness t with the attenuation length Λ', the intensity from the sample, given by (2), will be reduced to

$$N = K \cdot \exp\left(-\frac{t}{\Lambda'}\right). \tag{4}$$

If the contamination layer contains the same element as the underlaying sample, viz. carbon, its intensity contribution N' will be

$$N' = I_0 \cdot \Lambda'(E_{\text{kin}}) \cdot \varrho' \cdot A \cdot \frac{d\sigma}{d\Omega} \cdot \Omega \cdot D(E_{\text{kin}}) \left[1 - \exp\left(-\frac{t}{\Lambda'}\right)\right]$$
$$= K' \cdot \left[1 - \exp\left(-\frac{t}{\Lambda'}\right)\right] \tag{5}$$

where the primed symbols refer to the contamination layer. If all carbon analyzed were contained in the contamination layer, the intensity of the Mg 2*s* signal from the underlying MgO must decrease with increasing thickness t of the contamination layer according to (4).

In Fig. 1a the calculated Mg 2*s* decrease is plotted versus N'/K' from (5b) for various values of t. At C 1*s* intensities which would correspond to an overlayer of $t = 1.4$ nm, the Mg 2*s* intensity is expected to decrease by 30–40%. In Fig. 1b we have plotted the actually measured Mg 2*s* intensities from all our experiments versus the ratio of the measured C 1*s* intensities to the C 1*s* intensity from an infinitely thick overlayer. This is again equal to N'/K'.

Even for the highest C 1*s* intensities measured which are in excess of what one would expect for a 3–4, monolayer thick contamination layer, no downward trend of the Mg 2*s* intensity is noted. This shows that at least the majority of the carbon which contributes to the C 1*s* intensity is *not* contained in a contamination layer but in the MgO itself. Specifying that the word "surface" means the very last atomic layer and any contamination on top of it we can say that most of the carbon analyzed resides in the subsurface zone of the MgO crystal.

This point can be further substantiated by isothermal desorption measurements at 625 K of hydrocarbons from the purposely contaminated Cu support, as shown by Fig. 2a: the C 1*s* intensity decreases fast to a low level which can hardly be reduced further by either sputtering or heating. Probably the Cu support used in our experiments contained traces of dissolved carbon. In comparison to this low residual C 1*s* intensity from the Cu the C 1*s* intensity from the MgO crystal, recorded at the same temperature under the same condition could not be reduced thermally to a similarily low level but remained high as shown by Fig. 2b. After sputtering the C 1*s* signal was low but increased in a systematic manner while the Mg 2*s* intensity remained constant.

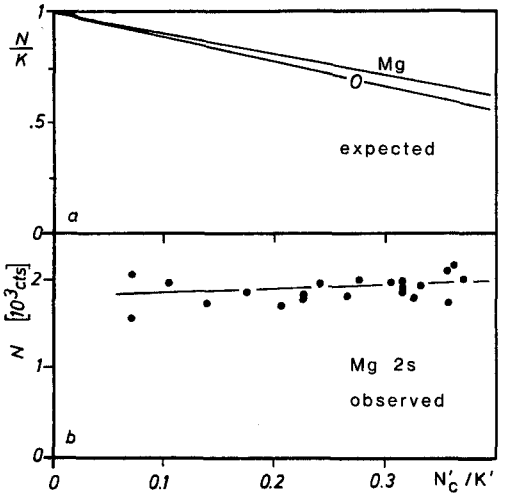

Fig. 1. (a) Attenuation of the Mg 2*s* signals from MgO surface, if it were covered by a contamination layer, as a function of the C 2*s* intensity. (b) Plot of the Mg 2*s* intensities versus the C 1*s* intensity as measured from MgO under a variety of experimental conditions

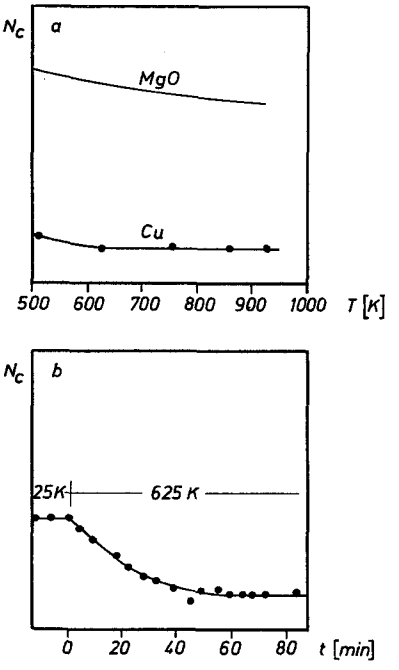

Fig. 2. (a) Typical C 1*s* signal intensities recorded from MgO and the blanc Cu support. (b) Typical desorption behavior of a hydrocarbon contamination layer from the Cu support at 625 K

2. Results

2.1. Carbon

Figure 3 shows the complex C 1*s* spectrum from MgO and its distinguishable components:

(a) The crystal C 1*s* signal as recorded from the MgO single crystal kept overnight at 500 K in the ultrahigh vacuum after having been sputtering with Ar^+ ions,

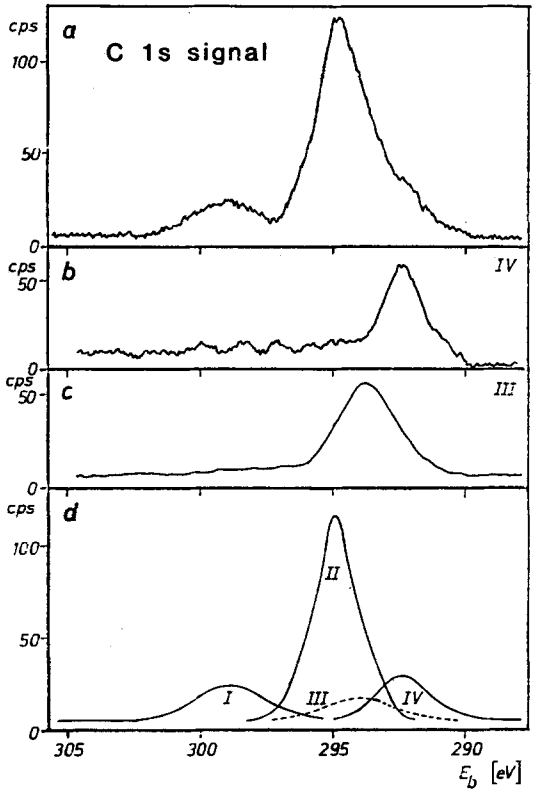

Fig. 3. (a) Complex C 1*s* spectrum as recorded from MgO at 500 K. (b) C 1*s* signal from the Cu support. (c) C 1*s* signal from a purposely adsorbed contamination layer on MgO. (d) Deconvolution of spectrum a into four components

(b) a C 1*s* peak III recorded from a Cu blank at 500 K,

(c) the C 1*s* peak IV recorded with reduced sensitivity and at 300 K from a MgO crystal which was purposely exposed to a high level of hydrocarbons in the residual gas,

(d) the deconvoluted C 1*s* spectrum featuring two more C 1*s* components, labelled I and II, at $E_b^{\mathrm{I}} = 298.8$ eV and $E_b^{\mathrm{II}} = 294.8$ eV, which belong neither to the Cu support nor to a contamination overlayer.

By sputtering the intensity of the C 1*s* signal II can be very much reduced while that of the components I, III, and IV less affected, unless the sample was contaminated and the C 1*s* IV intensity was high. After sputtering, upon isothermal annealing, the C 1*s* signal II increases, but signals I, III, and IV remain essentially constant.

This is shown in Fig. 4 for runs performed at 625, 730, and 925 K. The abscissa is in hours. As mentioned above, sputtering was done at 300 K and the time needed to achieve isothermal conditions was less than four and ten min to reach 730 and 925 K, respectively. The increase of the signal II continued over much longer time. It was the faster the higher the temperature. Eventually a steady value was reached which we shall call "saturation value". It is a function of the temperature: the higher the temperature, the lower the saturation value.

In Fig. 5 the saturation values are plotted as a function of temperature. The ordinate is shown in units of C/O giving the number of carbon atoms per oxygen of the MgO, as determined from the C 1*s* II intensity by (2) neglecting matrix effects. The highest C concentration in the analyzed layer is of the order of one C per two O.

The saturation values can be approached from either higher or lower temperatures. If the temperature is first set for sufficiently long time at, for instance, 925 K and then decreased to 730 K, the same saturation value is achieved within experimental error as if the sample were heated from 300 K. Expect for lower temperatures, where the C/O vs. T curve in Fig. 5 is shown as a dotted line, the saturation values are fully reversible. This behavior therefore suggests that they are equilibrium values. The fact that the C 1*s* I peak intensity does not increase as markedly as C 1*s* II as a function of time rules out a shake-up or shake-off origin. The shift is too large for a multiplet splitting caused by unpaired electrons. In some experiments we have noted an initial rapid rise of the C 1*s* I intensity suggesting that this peak might be due to a surface species which reaches very fast an equilibrium concentration. This species should be $\delta+$ with respect to that which causes the C 1*s* II peak.

2.2. *Oxygen*

The O 1*s* peak can be resolved into two components I and II yielding peaks at $E_b^{\mathrm{I}} = 541.0$ and $E_b^{\mathrm{II}} = 538.8$ eV, as shown by Fig. 6. The O 1*s* signal was split already before sputtering. Sputtering only increased the overall intensity of the O 1*s* peak. At 300 K the intensity of component I is allmost is allmost identical to that of component II, but decreases by a factor of about 2 during heating to 925 K. The O 1*s* II intensity remains essentially constant. Back at 300 K, the O 1*s* signal regains its high intensity over a period of about 10 h.

2.3. *Magnesium*

The Mg 2*p* and Mg 2*s* signals show only very little time- and temperature-dependent variations in their intensities as evidenced by Fig. 2. They did not develop any splitting or noticeable assymmetry as a result of sputtering.

3. Discussion

3.1. *Two Oxygen Species*

We assign the O 1*s* peak I at the higher binding energy to the oxygen species O^- as distinct from the usual

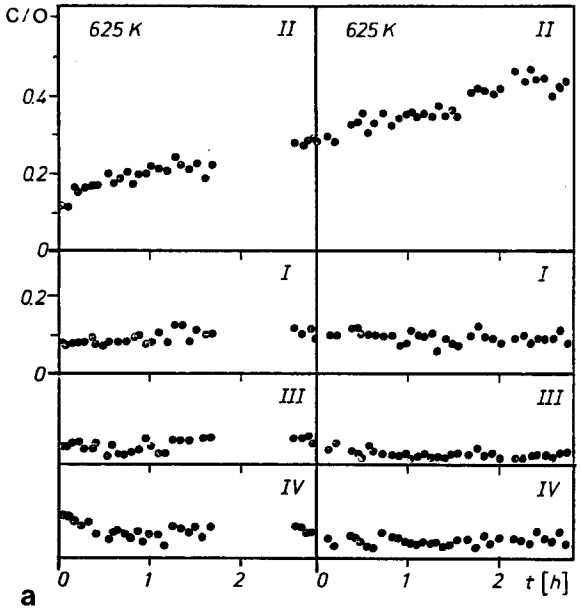

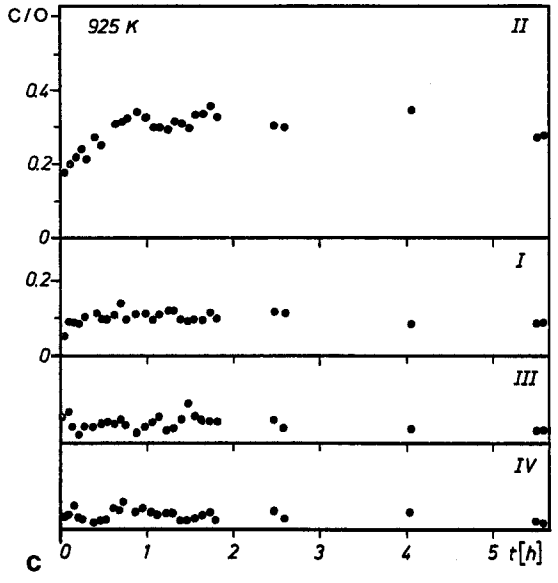

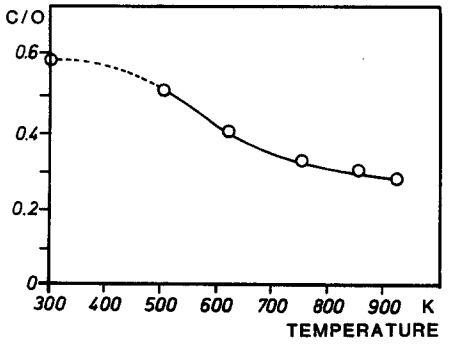

Fig. 5. Steady state concentration of the C^{II} species attained after long isothermal heating as a function of temperature

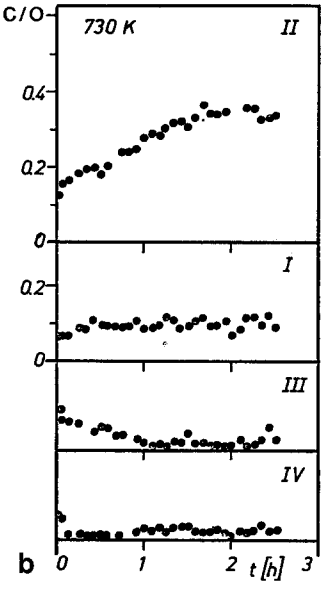

Fig. 4 (a) Intensity changes of the C 1*s* components from MgO, freshly sputtered, during isothermal heating at 625 K. (b) Intensity changes of the C 1*s* components from MgO, freshly sputtered, during isothermal heating at 730 K. (c) Intensity changes of the C 1*s* components from MgO, freshly sputtered, during isothermal heating at 925 K

O^{2-} of the MgO structure [12]. The high O 1*s* peak I intensity after sputtering can be attributed to partial oxidation of the surface combined with selective sputtering. The O 1*s* peak I decreases during heating, especially upon approaching 900 K, in agreement with the thermal instability of intermediate peroxy anions [13]. The fact that the O 1*s* peak I intensity increases again upon 300 K annealing can be attributed to the trapping of defect electrons from the bulk in the surface. This effect can be understood on the basis of the argument that at the surface the lattice energy is lowered with respect to the bulk lattice energy by a factor of the order of 1/2 the Madelung constant. This destabilizes the O^{2-} state.

3.2. *Dissolved Carbon*

It has been shown earlier by using the $^{12}C(d,p)^{13}C$ nuclear reaction that MgO single crystals, grown by arc-fusion and rated high purity with respect to their metal impurity content, contain dissolved carbon [1–4]. This carbon is characterized by a high mobility, a high reactivity [6, 7], and a strong tendency to become enriched in a subsurface zone which extends approximately 1 μm into the bulk. The (d,p) method has a depth resolution not better than ±0.2 μm. For

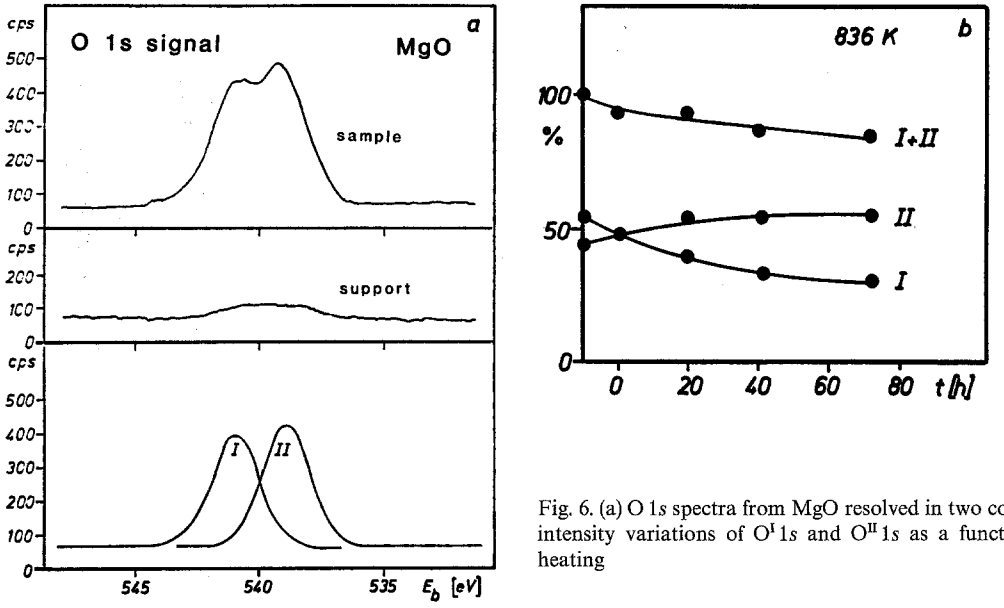

Fig. 6. (a) O 1s spectra from MgO resolved in two components I and II. (b) Relative intensity variations of $O^{I}1s$ and $O^{II}1s$ as a function of time during isothermal heating

MgO crystals containing typically 200–2500 at.-ppm C, corresponding to 0.2–2.5 carbon atoms per 1000 oxygen, the mean C concentration in the 0–0.5 μm subsurface layer was found to be of the order of 0.5–1 wt.-% or 15000–30000 at.-ppm [4], i.e. 1.5–3 carbon atoms per 100 oxygen. In other words, the carbon is enriched in the 0–0.5 μm subsurface zone by a factor of 10–100 with respect to the bulk.

The XPS data presented in this study show that the carbon enrichment continues to the topmost subsurface layer and reaches values as high as 50 carbon atoms per 100 oxygens or 2 carbon atoms per unit cell MgO, corresponding to an enrichment factor of the order of 1000 or even higher. On a relative scale the concentration values derived from the XPS data are probably correct within ±20%. The error in the absolute values may be larger, because, with reference to (2), the mean loss-free escape depth of the photoelectrons from the MgO and from the graphite single crystal is not known. As indicated above an error as large as by a factor of 2 appears possible. An error larger than by a factor of 4 can be excluded. Even assuming the most unfavorable case the carbon concentration in the analyzed layer would amount to about 10–20 carbon atoms per 100 oxygens.

The XPS data strongly suggests that the carbon concentration in this extremely C-enriched subsurface layer is a reversible function of the temperature. They thus support the conclusion derived earlier from the (d, p) measurements [1–4] that the carbon concentration depth profile in MgO adjusts reversibly to the temperature, being steep at low temperatures but extending further into the bulk at high temperatures.

Furthermore the XPS data confirm the earlier conclusion that the carbon species which segregate into the subsurface zone are extremely mobile considering the fact that in MgO the O^{2-} anions are densely packed with the Mg^{2+} cations occupying all octahedral voids.

The atomic size of the carbon is large in comparison to the size of the tetrahedrally coordinated interstitial sites, the only sites which are intrinsically unoccupied in the NaCl-type, face-centered cubic MgO structure. The possible reason for the observed subsurface carbon segregation has already been discussed in the earlier paper [4]. Local strains associated with the carbon species are believed to provide the driving force for the up-hill diffusion from regions of low C concentration in the bulk into the elastically relaxed, C-enriched subsurface zone. Conversely, with increasing temperature, the bulk relaxes to some extent and the carbon species diffuse back into the bulk down-hill the steep subsurface carbon concentration gradient, until a new equilibrium state is reached.

3.3. *Carbon Subsurface Profile*

The XPS and (d, p) data can be combined to derive the "best" carbon profile. Using the available values we can plot the carbon concentration versus the depth as shown in Fig. 7. Let us assume that the topmast layer analyzed by XPS to a depth of 5 nm contains typically 50 carbon per 100 oxygen, but averaged over the whole 0.5 μm thick layer analyzed by the (d, p) method the value is 3 carbon per 100 oxygen. For the next layer, 0.5–1.0 μm, we have from (d, p) measurements typically

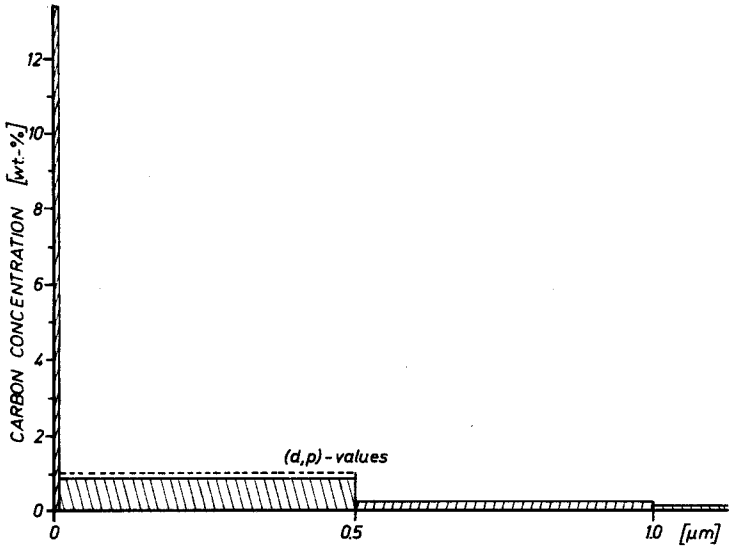

Fig. 7. Carbon concentration versus depth as calculated from XPS-data and (d, p)-data

1 carbon per 100 oxygen, and beyond 1.0 μm the bulk value is reached: 0.1 carbon per 100 oxygen, corresponding to about 300 wt.-ppm. We know that the extremely C-enriched zone to which the XPS value applies extends at least to a depth of 5 nm. Then for the next layer, 5 nm–0.5 μm, the (d, p) value has to be corrected: it can now contain only 2.5 carbon per 100 oxygen instead of 3. If we assume that the XPS value applies to a layer of 30 nm thickness, all carbon analyzed by the (d, p) method for the 0–0.5 μm layer would be contained in these topmost 30 nm and the next layer, 30 nm–0.5 μm, would be exempt of carbon. This is physically unreasonable, because we know that in the next layer, 0.5–1 μm, the average C concentration is again of the order of 1 carbon per 100 oxygen. We take 10 nm as the "best" value for the thickness of layer to which the XPS values apply.

3.4. *Evaluation of the Carbon Diffusion Coefficient*

When the surface of the MgO crystal is removed to a certain depth by argon ion sputtering, the carbon concentration in the topmost layer is lowered. Consequently, upon isothermal annealing, carbon will diffuse from the bulk normal to the surface.

In order to derive an expression for the diffusion coefficient we split the chemical potential μ into a bulk chemical potential μ_b and a surface chemical potential μ_s. Equilibrium requires that $\mu_b = \mu_s$. This is indicated schematically in Fig. 8a showing a section through the crystal from the surface to the bulk with an equilibrium carbon concentration profile. By sputtering away a surface layer of thickness Δz the C profile is cut off (Fig. 8b) and the surface chemical potential is lowered to μ_s^0. As a function of time the C profile rebuilds (Fig.

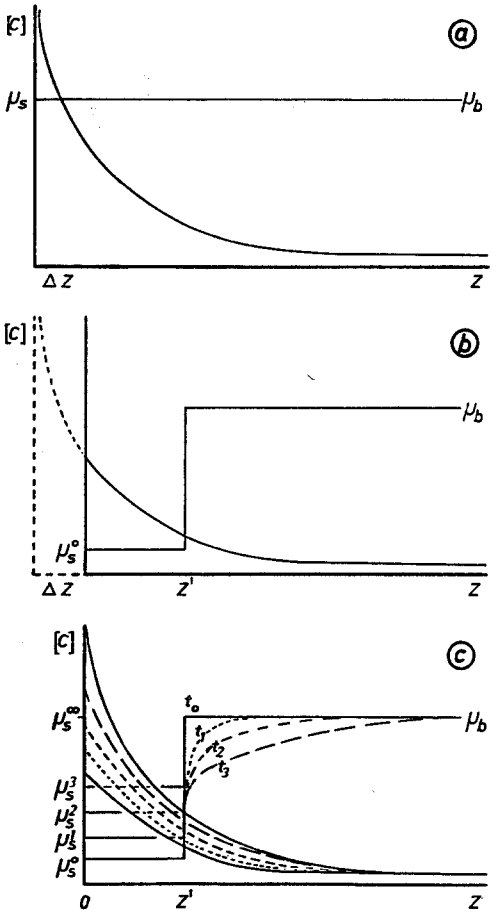

Fig. 8. (a) Carbon concentration profile and chemical potential as a function of depth. (b) Carbon concentration profile and chemical potential as a function of depth after sputtering. (c) Carbon profile and surface chemical potential as a function of time during isothermal heating

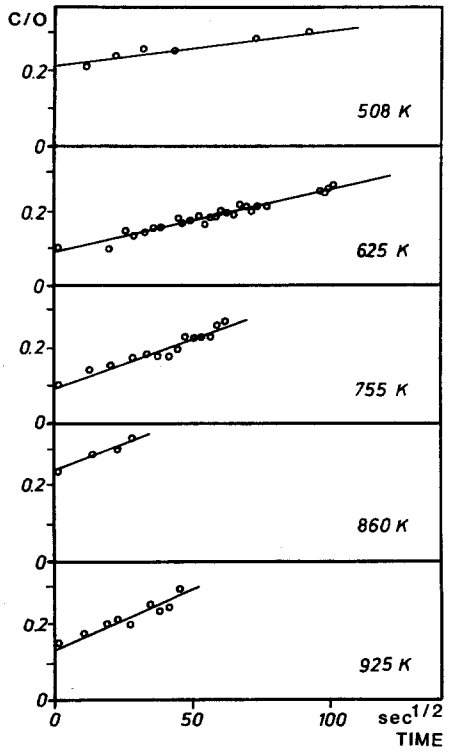

Fig. 9. Plot of the carbon concentration versus $\sqrt{t}$ during isothermal heating after sputtering

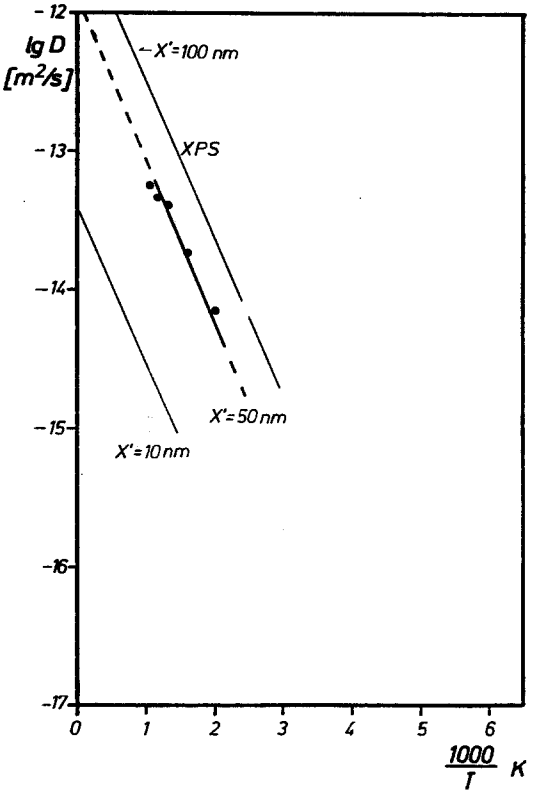

Fig. 10. Arrhenius plot of the diffusion coefficient calculated from XPS data versus $1/T$

8c) and the surface chemical potential goes from μ_s^0 to μ_s^1, $\mu_s^2 \ldots \mu_s^\infty$ which is again the equilibrium value.

The diffusion equation which describes this process can be solved, if we assume a rectangular trough as shown in Fig. 8 of depth z' and a linear relationship between μ_s and the C concentration increase. Then the carbon atoms diffusing from the bulk normal to the surface pass through the plane at z' and fill the through according to the 1-dimensional diffusion equation [14]:

$$C(z) = \frac{C_0}{1+k}\left[1 + k \cdot \mathrm{erfc}\left(\frac{z}{2} \cdot \sqrt{Dt}\right)\right], \tag{6}$$

where $C(z)$ is the C concentration as a function of z, C_0 is the excess C concentration in the bulk over that in the surface at $t=0$, t is the time, D is the diffusion coefficient and k a constant which depends upon μ_b and μ_s. erfc stands for $(1-\mathrm{erfc})$ where erf is the error function.

The number N of carbon atoms filling the trough is obtained by integrating:

$$N = \int_{z'}^{\infty} (C_0 - C_z)\, dz, \tag{7}$$

$$= \int_{z'}^{\infty} \frac{k \cdot C_0}{1+k} \cdot \mathrm{erfc}\left(\frac{z}{2} \cdot \sqrt{Dt}\right) dz. \tag{8}$$

For short times we may rearrange to

$$N = \frac{2k \cdot C_0}{1+k} \cdot \sqrt{Dt} \cdot \int_{z'}^{\infty} \mathrm{erfc}\, z'\, dz. \tag{9}$$

With $\int \mathrm{erfc}\, z'\, dz = 1/\pi$ this simplifies to

$$N = \frac{2k \cdot C_0}{(1+k)\pi} \cdot \sqrt{Dt}. \tag{10}$$

Assuming k to be large, $k/(1+k) \approx 1$ and we obtain

$$N \frac{2C_0}{\pi} \sqrt{Dt}. \tag{11}$$

By plotting the initial C concentration increase as measured by XPS versus $\sqrt{t}$ straight lines should be obtained with the slope $2C_0/\pi\sqrt{D}$. Figure 9 shows that this relationship is rather well fulfilled for all isothermal XPS measurements. The diffusion coefficient is: $D = D_0 \exp(-E/RT)$ where D_0 is the diffusion coefficient at infinitely high temperature T, E the activation energy and R the gas constant. In keeping with the arguments given above we choose a trough depth of 10 nm as the "best" value and we obtain the Arrhenius plot of Fig. 10 and numerically:

$$D_{\mathrm{C/MgO}} = 2 \times 10^{-9} \exp\left(-\frac{22.5}{RT}\right) \frac{\mathrm{cm}^2}{\mathrm{s}}; \quad \frac{\mathrm{kJ}}{\mathrm{mole}}.$$

If the trough depth were chosen to be 5 nm, D_0 would decrease by a factor of about 3. Probably the D_0 value given above is correct within one order of magnitude and the activation energy within ± 2.5 kJ/mole.

3.5. *Surface Stoichiometry*

It is well known from other oxides that sputtering may significantly change either the reduction state or the stoichiometry of the surface near region. In the case of MgO a reduction of the cation is unlikely. As mentioned in Sect. 4.3 the Mg 2*s* and Mg 2*p* signals did not show evidence of any splitting induced by sputtering. Also the fact that the O 1*s* signal was composed of two separate components I and II, appears not to be a result of sputtering. It cannot be ruled out that selective evaporation of Mg occurred thermally from the MgO surface which may be enhanced by sputtering. Any change in stoichiometry of the subsurface zone due to sputtering is expected to affect the C diffusion. One might suspect that the low activation energy for C diffusion reported here is a result of a change in stoichiometry in the subsurface zone, may be introduced by the sputtering procedure. This, however, is most certainly not the case, because essentially the same activation energy has been obtained, without sputtering, from acid-etched MgO single crystals by means of the $^{12}C(d,p)^{13}C$ method [12] where the depth range analyzed extends to about 2 μm [16].

Conclusions

It has been possible to separate surface contamination from carbon contained in the subsurface layer of MgO and to construct a carbon concentration depth profile by combining the XPS data with earlier results obtained by the $^{12}C(d,p)^{13}C$ method [4]. The earlier presumption was confirmed that the carbon dissolved in MgO is extremely mobile and tends to segreate into the elastically relaxed subsurface zone but to redissolve in the bulk at higher temperatures. The C concentrations reversibly achieved in the topmost layers are extremely high, up to approximately one carbon per two oxygen or two carbon atoms per unit cell MgO. The diffusion coefficient which was derived from kinetic XPS data was found to be high and characterized by a low activation energy. This is quite surprising for carbon atoms which are not particularily small atomic species. On the other hand, the MgO structure is dense. Only its tetrahedrally coordinated interstitial sites are empty and available for the diffusing carbon species. Probably the diffusion is linked to O^- which represent defect electrons in the O^{2-} matrix of the MgO [15] and which form delocalized covalent bonds with the carbon [12].

Acknowledgements. This work was supported in part by grants from the "Deutsche Forschungsgemeinschaft", Bonn. Purchase of the MgO single crystals was made possible by a grant from the Freunde und Förderer der Universität zu Köln, Köln. Dr. G. Wolff, KFA Jülich, kindly analyzed the carbon content of the samples.

References

1. F. Freund, G. Debras, G. Demortier: J. Cryst. Growth **38**, 277–80 (1977)
2. F. Freund, G. Debras, G. Demortier: J. Am. Ceram. Soc. **61**, 429–434 (1978)
3. F. Freund, H. Kathrein, H. Wengeler, R. Knobel, G. Demortier: Mater. Res. Bull. **15**, 1011–1018 (1980)
4. H. Wengeler, R. Knobel, H.Kathrein, G. Demortier, G. Wolff, F. Freund: J. Phys. Chem. Solids **43**, 59–71 (1982)
5. F. Freund, R. Knobel, H. Wengeler, H. Kathrein, G. Oberheuser, R.G. Schäfer: Geol. Rundschau **71**, 1–21 (1982)
6. R. Knobel, F. Freund: Mater. Res. Bull. **15**, 1247–1253 (1980)
7. F. Freund, R. Knobel, G. Oberheuser, G.C. Maiti, R.G. Schäfer: Mater. Res. Bull. **15**, 1385–1391 (1980)
8. G. Deconninck: *Introduction to Radioanalytical Physics*, Nuclear Methods Monographs 1 (Elsevier, Amsterdam, Oxford, New York 1978)
9. D.T. Clark, H.R. Thomas, A. Dilks, D. Shuttleworth: J. Electron. Spectrosc. Relat. Phenom. **10**, 455–460 (1977)
10. C.S.V. Fadley: In *Electron Spectroscopy – Theory, Techniques and Applications*, Vol. 1, ed. by C.R. Brundle, A.D. Baker (Academic Press, London, New York, San Francisco 1977)
11. H. Kathrein: Ph. D. Thesis, University Cologne
12. F. Freund: Contrib. Mineral. Petrol. **76**, 474–482 (1981)
13. R. Martens, H. Gentsch, F. Freund: J. Catalysis **44**, 366–372 (1976)
14. J. Crank: The Mathematics of Diffusion (Clarendon Press, Oxford 1957)
15. H. Kathrein, F. Freund: J. Phys. Chem. Solids (in press) (1982)